Deformation and Slip Along the Sunda Megathrust in the Great 2005 Nias-Simeulue Earthquake

Richard W. Briggs,[1*] Kerry Sieh,[1] Aron J. Meltzner,[1] Danny Natawidjaja,[2] John Galetzka,[1] Bambang Suwargadi,[2] Ya-ju Hsu,[1] Mark Simons,[1] Nugroho Hananto,[2] Imam Suprihanto,[3] Dudi Prayudi,[2] Jean-Philippe Avouac,[1] Linette Prawirodirdjo,[4] Yehuda Bock[4]

Seismic rupture produced spectacular tectonic deformation above a 400-kilometer strip of the Sunda megathrust, offshore northern Sumatra, in March 2005. Measurements from coral microatolls and Global Positioning System stations reveal trench-parallel belts of uplift up to 3 meters high on the outer-arc islands above the rupture and a 1-meter-deep subsidence trough farther from the trench. Surface deformation reflects more than 11 meters of fault slip under the islands and a pronounced lessening of slip trenchward. A saddle in megathrust slip separates the northwestern edge of the 2005 rupture from the great 2004 Sumatra-Andaman rupture. The southeastern edge abuts a predominantly aseismic section of the megathrust near the equator.

A giant megathrust earthquake is the rare expression of the most dramatic moment of a subduction zone's life cycle—the culmination of centuries of strain accumulation across a convergent plate boundary. Robust seismic signals around the globe allow estimation of the gross nature of the event, but the details of rupture are usually obscure due to a lack of geodetic measurements directly above or nearby.

The great [moment magnitude (M_w) = 9.2] Sumatra-Andaman earthquake of December 2004 (Fig. 1) was unusual for a subduction megathrust event in that geodetic measurements of coseismic motions were available from islands directly above the rupture (*1*). These near-field data enabled a detailed investigation of the source of the earthquake. Even so, near-field Global Positioning System (GPS) geodetic measurements were sparse. Furthermore, they were collected in survey mode, with long periods between measurements that led to ambiguities in separating pre-, co-, and postseismic motions.

The great (M_w = 8.7) Nias-Simeulue earthquake, 3 months later and immediately to the south (Fig. 1), presents a substantially better opportunity to constrain rupture processes. Several continuously recording GPS (CGPS) stations had just been established directly above or immediately adjacent to the rupture (*2*). Moreover, the presence of a tropical archipelago above the rupture enabled the use of coral microatolls to measure coseismic uplift and submergence. The resulting rich set of measurements allows us to construct one of the most detailed and accurate maps of deformation obtained for a subduction megathrust earthquake.

Methods. Most of our measurements come from massive corals of the genus *Porites*. Because these are sensitive natural recorders of lowest tide levels (*3*–*5*), they are ideal natural instruments for measuring emergence or submergence relative to a tidal datum. Massive *Porites* coral heads grow radially upward and outward until they reach an elevation that exposes their highest corallites to the atmosphere during lowest tides. This subaerial exposure kills the uppermost corallites in the colony, thus restricting future upward growth. Hence the coral heads provide an opportunity to measure the difference between the highest level of survival (HLS) formed just before and that formed just after a large uplift event (*4*, *6*) and even to extract interseismic histories of vertical deformation (*7*, *8*).

When coseismic uplift occurs, those portions of the microatoll colony raised above lowest tides die. But if lower parts of the coral head are still below lowest tides, its uppermost living tissues demarcate a new, post-earthquake HLS (*4*) (Figs. 2A and 3A). Most of our uplift measurements are derived from the difference between pre- and post-earthquake HLS, often on the same coral head. Where corals rose during both the 2004 and 2005 earthquakes, we can differentiate between the two uplifts (Figs. 2A and 3B).

At locations where uplift was greater than the height of the coral heads and at sites that experienced subsidence (Fig. 2, B and C), we record the elevation difference between the coral's pre-earthquake HLS and average water level at the site at the time of our coral measurement. We then use a numerical tidal model to obtain an estimate of the lowest annual low tide expected at each survey site relative to the water level at the time of measurement. Our tidal calculations are based on harmonic tidal

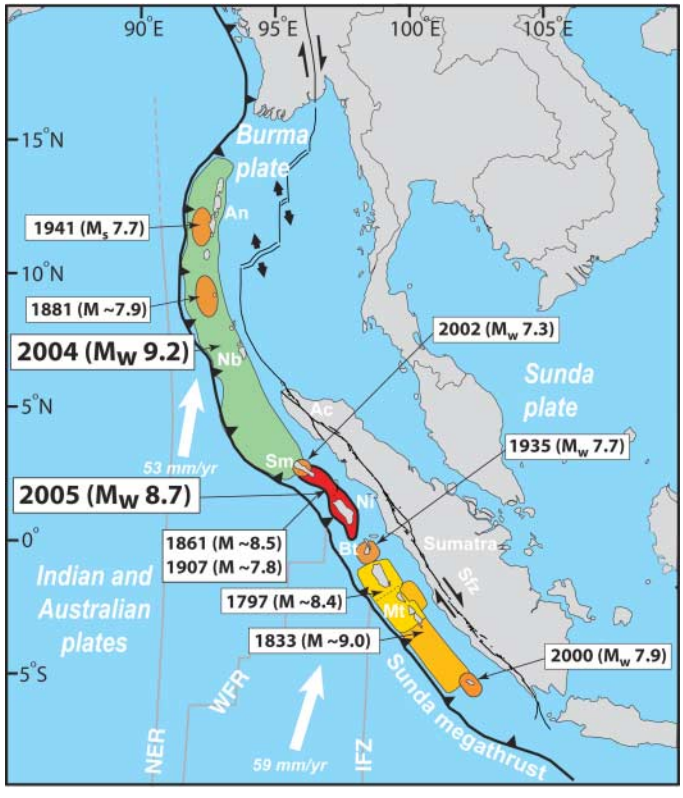

Fig. 1. Regional map of the 28 March 2005 rupture and previous large ruptures of the Sunda megathrust. The 2005 rupture occurred in a 400-km gap between great ruptures in 2004 and 1797. Islands above the rupture allowed detailed measurement of coseismic deformation with corals and GPS. An, Andaman islands; Nb, Nicobar islands; Ac, Aceh province; Ni, Nias island; Sm, Simeulue island; Bt, Batu islands; Mt, Mentawai islands; Sfz, Sumatran fault zone; NER, Ninety East ridge; WFR, Wharton fossil ridge; IFZ, Investigator fracture zone. Previous earthquake locations and magnitudes are from (*1*, *8*, *35*, *36*). Indian and Australian plate motions relative to Sunda are from (*37*) and faults are generalized from (*24*, *38*).

[1]Tectonics Observatory, Division of Geological and Planetary Sciences, California Institute of Technology, Pasadena, CA 91125, USA. [2]Research Center for Geotechnology, Indonesian Institute of Sciences, Bandung, Indonesia. [3]Jl. Mahoni, Blok E, Gang I, No. 13, Rt. 002/015, Kota Jakarta 14270, Indonesia. [4]Cecil H. and Ida M. Green Institute of Geophysics and Planetary Physics, Scripps Institution of Oceanography, University of California San Diego, La Jolla, CA 92093, USA.

*To whom correspondence should be addressed. E-mail: briggs@gps.caltech.edu

constituents extracted from a regional satellite-based model for Indonesia (*9*), using the software package NLOADF (*10*, *11*). The uplift or subsidence value is the difference between the pre-earthquake HLS (old extreme low tide elevation) and the model value of post-earthquake lowest tide. Where we can directly compare post-earthquake HLS and post-earthquake tide elevations, we find that a band of living coral about 4 cm high can survive above the elevation of extreme low tide. Thus, we apply this correction to all measurements that use the tidal model (*12*).

At a few survey sites, coral records are unavailable. There we estimate uplift using geomorphic or cultural features. These measurements often have relatively large uncertainties, but they are still useful in that they offer unambiguous evidence of the direction of land-level change. We also augment our field measurements in a few locations with limits on uplift and subsidence derived from satellite imagery (table S1). Finally, we also use coseismic displacements recorded by CGPS stations of the Sumatran GPS Array (SuGAr) (*2*) and a station (SAMP) operated by the Indonesia National Coordinating Agency for Surveys and Mapping (BAKOSURTANAL). The CGPS data were analyzed (*13*) in 24-hour segments (0- to 24-hour GMT) with data from 10 additional continuous GPS sites on Java, Cocos Islands, Diego Garcia, Singapore, India, Australia, and Guam. These regional network solutions were combined by network adjustment with global GPS network solutions produced routinely at the Scripps Orbit and Permanent Array Center. The resulting 24-hour position time series were fit to estimate three-dimensional coseismic displacements (*13*).

Results. The northern half of Simeulue island, from about 2.5° to 2.9°N, rose during the December 2004 event (Fig. 4A; table S2). Tilts were toward the northeast and southeast, with maximum uplift of 1.45 m on the island's northwestern tip. The uplift of Simeulue constrains tightly the southeastern limit of megathrust rupture during the 2004 earthquake to about 2.5°N (*1*, *11*). The southeastern third of Simeulue subsided in December 2004, but we had little time to document that subsidence in the field before the subsequent March event. We have only a few field measurements from January 2005 and observations from satellite imagery (*11*), as well as the subsidence predicted from an elastic dislocation model of the 2004 rupture (*1*). Rather than apply these largely model-derived corrections to our measurements of March 2005 uplift on southeastern Simeulue, we contour net uplift values for sites that subsided in the 2004 earthquake (Fig. 4B). Moreover, measurements by CGPS show that the postseismic elevation changes by the time of our field survey, 1.5 to 3.2 months after the earthquake, were only rarely more than a few percent of total coseismic motion (fig. S1). Therefore, we have chosen not to include corrections for these relatively small postseismic motions in our depiction of coseismic deformation. Instead, we leave close examination of pre- and post-earthquake deformation to a subsequent manuscript (*14*).

The vertical deformation pattern of March 2005 comprises principally two arc-parallel ridges of uplift on the forearc islands of Nias and Simeulue and a broad subsidence trough between these islands and the mainland coast (Fig. 4B). This pattern—uplift nearer the deformation front and subsidence nearer the arc (fig. S2)—is like that observed after a few other megathrust ruptures, principally in Alaska, Chile, and Japan (*15*–*18*). The asymmetry of the pattern, with maximum uplift (2.9 m) greater than maximum subsidence (1.15 m), is also similar to the patterns in these previous cases. The ridge crests are sharper than the trough. The contours of uplift and subsidence are predominantly arc-parallel, but have a pronounced misalignment near the Banyak Islands, between Nias and Simeulue.

Modeling. We combine our coral observations with coseismic three-component displacements from 16 CGPS stations of the SuGAr network to constrain an elastic dislocation model of coseismic slip on the megathrust (Fig. 5). To construct the model, we assume a 10° dipping

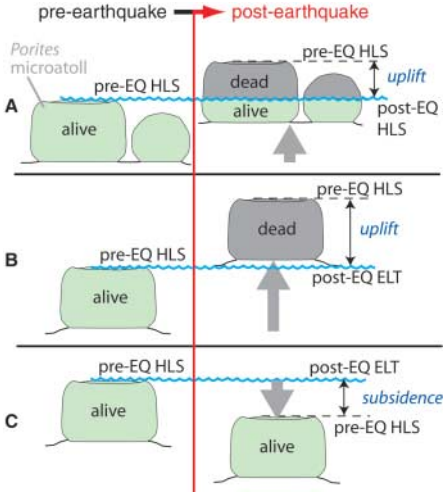

Fig. 2. Three scenarios for measuring vertical deformation using *Porites* coral microatolls. (**A**) Uplift recorded as the difference between pre- and post-earthquake highest level of survival (HLS). (**B**) Uplift as separation between pre-earthquake HLS (pre-EQ HLS) and the model elevation of post-earthquake extreme low tide (post-EQ ELT). (**C**) Subsidence measured upward from pre-earthquake HLS to post-earthquake ELT.

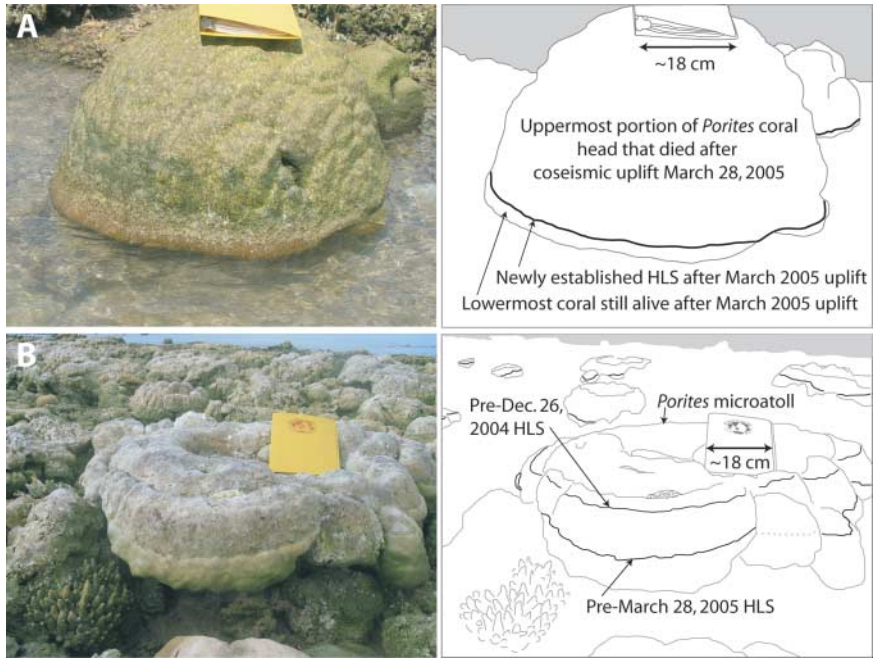

Fig. 3. Photographs and corresponding line drawings of uplifted *Porites* coral heads. (**A**) An uplifted hemispherical *Porites* head that records the new, post-earthquake highest level of survival (HLS) as the top of a thin living strip at its base. The uppermost, exposed portion of the microatoll is dead and covered with algae (site RDJ05-K; table S2). (**B**) A *Porites* microatoll that records multiple uplift events. Uplift of ~11 cm during the December earthquake resulted in the elevation difference between the uppermost living coral before (labeled "Pre-Dec. 26, 2004 HLS") and after ("Pre-March 28, 2005 HLS") the earthquake. The more brightly colored area beneath the pre–28 March 2005 HLS is outward growth during the period between the December and March earthquakes. During the 28 March earthquake the coral was uplifted another ~65 cm, causing the head to be lifted entirely out of the water into a position too high to record post–28 March HLS (site RND05-C; table S2).

fault plane between the deformation front and offshore Sumatra, which conforms roughly to the top of the Wadati-Benioff zone defined by relocated hypocenters from the International Seismological Centre catalog (*19*, *20*). We curve the fault along strike to follow the trench and use a layered elastic structure derived from the crustal model CRUST2.0 (*21*). Models with greater geometrical complexity will not be warranted until the geometry of the megathrust and crustal density structure are better known. Our weighted least-squares approach uses data weights equal to the inverse square root of the data covariance matrix (*22*). We estimate appropriate relative weight between the GPS and coral data in a two-step process. We begin by constructing two independent models that use each data set separately. The final model uses both data sets simultaneously, but with the weight of each data set scaled by the reduced chi-square values inferred from the initial independent models. In this joint inversion, fits to the vertical CGPS and the coral data are generally very good (*22*) (figs. S3 to S7).

Inverting the coral and CGPS data for slip on the megathrust yields a band of high slip that stretches from 3°N to the equator (Fig. 5). The region of high slip comprises two main patches, one northwest and one southeast of the epicenter. Maximum slip near southern Simeulue is about 8 m, whereas under northern Nias it is about 11 m. Most of the moment (95%) is concentrated between depths of about 14 to 35 km. The surface projections of the slip maxima are about 10 km east of the belts of maximum uplift. Slip values are highest at depths of about 25 km and decrease gradually both up-dip and down-dip. The total moment of the rupture is 9.8×10^{21} N-m, nearly identical to the seismological estimate (*23*) and equivalent to $M_w = 8.6$.

Discussion. Our observations have implications for the segmentation of the megathrust and for its long-term behavior. First, we speculate on the importance of the misalignment of the coseismic deformation contours. The bend or tear in the contours between the Banyak islands and Nias (Fig. 4B) separates the two principal rupture patches. It also coincides with a disruption in the bathymetry of the outer-arc ridge, previously interpreted to be a structural tear, possibly the southwestward extension of the Batee fault (fig. S8). This fault offsets forearc geologic features dextrally as much as 90 km (*24*, *25*). We suggest that the misalignment of coseismic deformation contours demarcates a tear in the megathrust between the two principal patches of coseismic rupture. If this break in the megathrust exists, the dip of the megathrust to the northwest (beneath Simeulue) might well be shallower than it is to the southeast (beneath Nias), because the uplift ridge on Simeulue is farther from the trench than the uplift ridge on Nias.

The relationship of coseismic slip on the megathrust to bathymetry, aftershocks, and

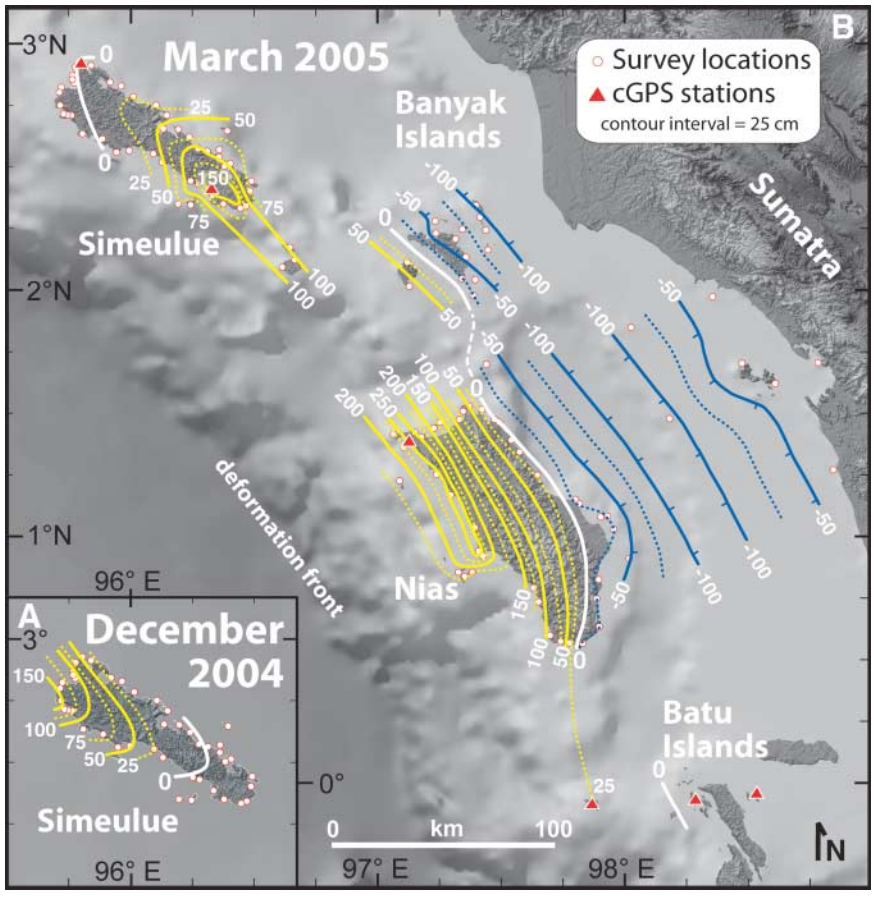

Fig. 4. Contour maps in cm of vertical deformation during the December 2004 (**A**) and March 2005 (**B**) Sunda megathrust ruptures. Yellow contours indicate uplift, blue contours indicate subsidence, and the white contour is the pivot line between domains of uplift and subsidence. Solid contours are at 50-cm interval, and dashed contours are at 25-cm interval. The principal features are two ridges of uplift along the islands of Nias and Simeulue and troughs of subsidence between the islands and the mainland. Shaded relief is from (*39*, *40*).

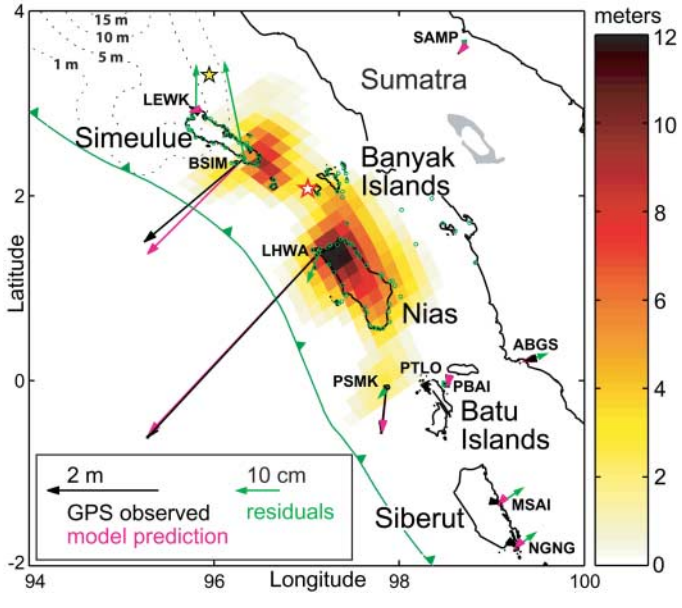

Fig. 5. Map view of model coseismic slip distribution on the 28 March 2005 Nias-Simeulue fault plane. Horizontal displacements from CGPS are in black and model values are in pink. All CGPS sites are from the Sumatran GPS Array (SuGAr), except for site SAMP, which is operated by BAKOSURTANAL. Model residuals are shown as green vectors (note change of scale). Slip reached 8 m under Simeulue and 11 m under Nias. Green circles show locations of uplift measurements. The epicenter of the March 2005 mainshock is shown as a red star, and the green line denotes the position of the Sunda deformation front. Dashed contours show modeled slip for the 2004 Aceh-Andaman rupture from (*1*), and the yellow star denotes the epicenter of the 2004 mainshock.

postseismic slip has implications for the long-term behavior of the megathrust. It is interesting that the two high-slip patches seem to correspond to steep topography rising from the trench (Fig. 4B and fig. S9). Moreover, patches with low slip, between Nias and Simeulue island and under southern Nias island, are coincident with gentler slopes up from the trench. More reliable bathymetry will be necessary to confirm these associations. But if they are indeed correct, high-slip and low-slip patches may be features of the megathrust as long-lived as sea-floor topography. Perhaps the steep slopes have been built above sections of the megathrust with higher friction and the gentle slopes reflect sections of the megathrust with lower friction (*26*).

The coincidence of a dense band of aftershocks (*27*) (fig. S8) with the rapid up-dip decrease in slip just seaward of the islands suggests that stresses imposed by the coseismic rupture were high enough there to induce a concentration of aftershocks on or in the volume surrounding the shallower part of the interface. What prevented the rupture from progressing farther up-dip? Had the shallower part of the megathrust been de-stressed by coseismic rupture in the earlier large historical ruptures of 1907 or 1861? Or does aseismic slip keep the up-dip section de-stressed and unreceptive to the propagation of slip during 2005-like ruptures? Work in progress on postseismic transients recorded by the Sumatran GPS Array (*14*, *28*) addresses these possibilities.

Another interesting aspect of the March 2005 earthquake is the small size of the March 2005 tsunami relative to that of December 2004 (*29*, *30*). Most of the explanation for this difference must lie in a comparison of vertical sea-floor displacements generated during the two earthquakes. First, the length of rupture in March was much less—~400 km versus ~1600 km (*1*). Second, the maximum uplift in March was only about half that in December [2.9 m versus about 5.4 m (*31*)]. And third, the areas of greatest vertical displacement occurred under deep water along much of the December rupture, but on land or under shallow water along all of the March rupture. This third observation supports the calculation of Synolakis and Arcas (*30*), which shows that the presence of islands in the epicentral region substantially lessened the size of the March 2005 tsunami. Finally, the coseismic raising of Nias and Simeulue islands, tens of minutes before the arrival of the 28 March tsunami, would have resulted in a lessening of tsunami height and inundation along the upraised coasts of those islands (*29*, *32*).

It is clear from the cup shape of microatolls on the coasts of Nias and Simeulue that submergence associated with strain accumulation had been prevalent on the forearc in the decades before sudden uplift during the earthquake. This interseismic behavior, abruptly terminated by coseismic uplift, is consistent with slow elastic strain accumulation and abrupt release. Nonetheless, the fact that the pattern of coseismic uplift mimics the topography of the islands (Fig. 4B) suggests that some increment of the coseismic uplift is not elastic and has contributed to building of the outer-arc ridge. Indeed, the presence of well-preserved coral reef terraces tens of meters above sea level on the northern and central coasts of Nias island (*33*) attests to net uplift during the past few tens to hundreds of millennia. The coincidence of the coseismic pivot line with the boundary between long-term erosion (on the west) and deposition (on the east) further supports the argument that the coseismic pattern reflects long-term orogenic processes. The actual relative amounts of permanent and elastic components should be resolvable through a combination of paleogeodetic and neotectonic studies.

The lateral terminations of the March 2005 rupture are particularly interesting. The dense coral measurements on the coasts of Simeulue island allow us to examine the northwestern terminus in particular detail. Uplift during the 2004 earthquake was as high as 1.45 m on the northwestern flank of Simeulue island and tapered toward the southeast to zero (Fig. 4A). Conversely, uplift during the 2005 event was as high as 1.65 m on the southeastern part of the island and tapered toward the northwest nearly to zero (Fig. 4B). Summing uplifts from the two earthquakes reveals a 70-km-long saddle-shaped depression centered on the island (Fig. 6). At the center of this saddle, uplift was only ~0.5 m, at least a meter less than to the northwest and southeast. This implies that slip on the megathrust beneath central Simeulue was appreciably less than it was to the northwest and southeast. The corals also show that uplift associated with the M_w = 7.3 earthquake of 2002 (*34*) was centered squarely in the center of this saddle and had a maximum value of only ~0.2 m, an amount that is inadequate to fill the saddle (Fig. 6).

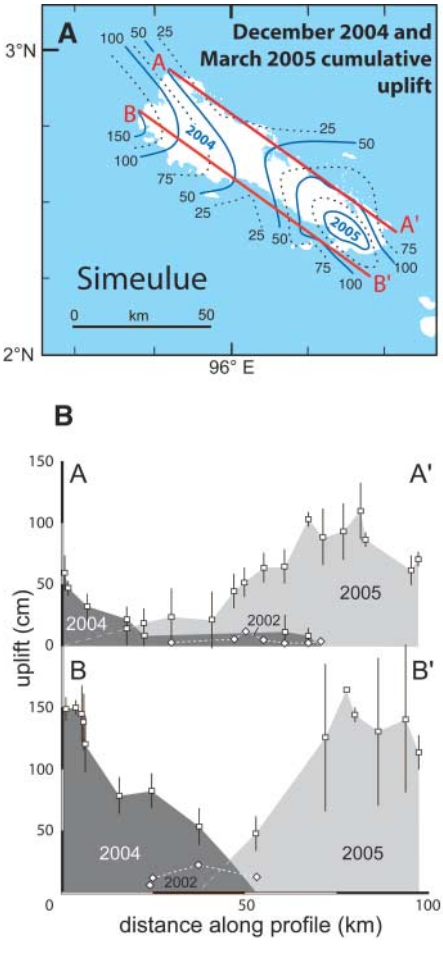

Fig. 6. Contour map of cumulative uplift values (in cm) for the December 2004 and March 2005 ruptures on Simeulue (**A**). Vertical displacement profiles A-A′ and B-B′ (**B**) highlight saddle in displacement between regions of December 2004 and March 2005 uplift. Measurements of uplift associated with the 2002 rupture appear as diamonds.

One plausible interpretation is that the Simeulue saddle reflects a section of the megathrust that commonly slips aseismically or fails in lesser earthquakes. Such a section could serve as an impediment to along-strike propagation of infrequent large ruptures. If slip in the long periods between giant earthquakes occurs largely aseismically and during moderate earthquakes such as occurred in 2002, this 70-km section would be largely unstressed at the time of the giant earthquakes and rupture would be less likely to propagate through. If this were a persistent characteristic of the Simeulue saddle, it would represent a permanent impediment to rupture from the northwest and from the southeast, because it would not accumulate large stresses. Such behavior could be analogous to that documented for the section of the Sunda megathrust at the Equator (*8*). This Batu islands section was flanked on the northwest by the giant ruptures of 1861 and 2005 and on the southeast by the giant earthquake rupture of 1797 (Fig. 1). Throughout at least the past 250 years, the M_w = 7.7 earthquake of 1935 is the largest seismic rupture of the 70-km-long Batu islands patch (*8*). Perhaps slip along the megathrust beneath the Batu islands, and the Simeulue saddle, is predominantly aseismic. The reasons for lateral variations in the mode of failure along the megathrust are unclear; abrupt lateral variations of temperature along the plate interface are improbable, so variations in the mode of slip along strike may instead result from lithologic or pore pressure variations. Another possibility is that structural complexities in the Simeulue saddle and Batu islands patch may have inhibited throughgoing rupture during the 2004 and 2005 giant earthquakes. The slight misalignment of the 2004 and 2005 uplift ridge crests on Simeulue island and the abrupt widening of the island at that misalignment, and the subduction of the Investigator fracture zone beneath the Batu islands zone, support arguments for a structural cause for the

2005 rupture terminations. These might be tears or warps in the megathrust or secondary faults within the slab or within the forearc.

References and Notes

1. C. Subarya *et al.*, *Nature* **440**, 46 (2006).
2. These CGPS data are available (www.tectonics.caltech.edu/sumatra/data.html and sopac.ucsd.edu/projects/sugar.html).
3. T. P. Scoffin, D. R. Stoddart, *Philos. Trans. R. Soc. London Ser. B* **284**, 99 (1978).
4. F. W. Taylor, C. Frohlich, J. Lecolle, M. Strecker, *J. Geophys. Res.* **92**, 4905 (1987).
5. J. Zachariasen, K. Sieh, F. W. Taylor, W. S. Hantoro, *Bull. Seismol. Soc. Am.* **90**, 897 (2000).
6. J. M. Pandolfi, M. M. R. Best, S. P. Murray, *Geology* **22**, 239 (1994).
7. K. Sieh, S. N. Ward, D. Natawidjaja, B. Suwargadi, *Geophys. Res. Lett.* **26**, 3141 (1999).
8. D. H. Natawidjaja *et al.*, *J. Geophys. Res.* **109**, B04306 (2004).
9. G. D. Egbert, S. Y. Erofeeva, *J. Atmos. Oceanic Technol.* **19**, 183 (2002).
10. D. C. Agnew, *J. Geophys. Res.* **102**, 5109 (1997).
11. A. J. Meltzner *et al.*, *J. Geophys. Res.* **111**, B02407 (2006).
12. We use principally a total station and an auto level and stadia rod to obtain field measurements. Total 2σ (95%) uncertainties associated with our coral measurements range from ± 6 to ± 23 cm and take into account variations in HLS, uncertainties in the tide model, survey measurement error, and uncertainties in the lowest low-tide to post-earthquake HLS correction.
13. R. Nikolaidis, thesis, University of California, San Diego (2002).
14. Y.-j. Hsu *et al.*, in preparation.
15. G. Plafker, *Science* **148**, 1675 (1965).
16. G. Plafker, J. C. Savage, *Geol. Soc. Am. Bull.* **81**, 1001 (1970).
17. T. J. Fitch, C. H. Scholz, *J. Geophys. Res.* **76**, 7260 (1971).
18. H. Kanamori, *Annu. Rev. Earth Planet. Sci.* **1**, 213 (1973).
19. E. R. Engdahl, R. van der Hilst, B. Raymond, *Bull. Seismol. Soc. Am.* **88**, 722 (1998).
20. This dip angle is slightly higher than the 7° northeast dipping plane of the Harvard centroid moment tensor solution for the main shock but is consistent with the 10° dip derived from modeling of teleseismic short-period and long-period seismic waveforms as well as normal modes (*23*).
21. C. Bassin, G. Laske, G. Masters, *EOS Trans. AGU* **81**, F897 (2000).
22. In our model we limit slip directions to be up-dip and right-lateral, and we minimize the data misfit and model roughness. The damping parameter between data misfit and model norm is chosen by cross-validation. To weight the GPS and coral data correctly, we first calculated two independent elastic-dislocation models, using each data set separately. The fact that the two solutions yield quite different reduced chi-square values (535 for the CGPS data and 10 for the coral data) suggests that the uncertainties assigned to the two independent data sets do not represent similar confidence levels. As a result, a joint inversion of the two data sets is dominated by the GPS measurements, which have far smaller errors. Thus, the joint inversion largely ignores the coral data, and the resultant slip model is strongly biased by the spatial distribution of the GPS stations. To remedy this bias, our final model is a joint inversion of both data sets with the weight of each data set scaled by the reduced chi-square value from the initial independent models. The rescaling factor between the CGPS data and the coral data is ~7. This procedure preserves the internal consistency of uncertainties assigned to each data set. It assumes that for each data set, real 1σ uncertainties are proportional to the initially assigned uncertainties (meaning that all sources of errors are assumed to be correctly accounted for in the estimated uncertainties). This combination of the two data sets takes appropriate advantage of the accuracy of the GPS measurements and of the dense spatial distribution of the coral measurements. To account for submergence due to the 2004 M_w = 9.2 rupture, our inversion uses a small elastic model–derived correction from Subarya *et al.* (*1*) (column m in table S2) that we apply to 2005 uplift values on southern Simeulue. The chi-square and weighted root-mean-squared values of the best-fit model are equal to 189 and 0.0497 m, respectively [based on 102 (coral) + 16 × 3 (CGPS) = 150 measurements].
23. A. O. Konca *et al.*, *Eos Trans. AGU* **86**, Abstract T31C-03 (2005).
24. D. E. Karig, M. B. Lawrence, G. F. Moore, J. R. Curray, *J. Geol. Soc. London* **137**, 77 (1980).
25. K. Sieh, D. Natawidjaja, *J. Geophys. Res.* **105**, 28,295 (2000).
26. D. Davis, J. Suppe, F. A. Dahlen, *J. Geophys. Res.* **88**, 1153 (1983).
27. Seismicity obtained from the National Earthquake Information Center (http://neic.usgs.gov/neis/epic/).
28. Y. Hsu *et al.*, *Eos Trans. AGU* **86**, Abstract T31C-02 (2005).
29. U.S. Geological Survey, "Notes From the Field…USGS Scientists in Sumatra Studying Recent Tsunamis: Leg 2 Reports, 12 April to 30 April 2005"; available at http://walrus.wr.usgs.gov/news/reports.html (2005).
30. R. A. Kerr, *Science* **308**, 341 (2005).
31. M. Chlieh, personal communication.
32. J. Borrero, B. McAdoo, paper presented at the International Meeting on the Sumatran Earthquake Challenge, Padang, Sumatra, Indonesia, 25 August 2005.
33. H. Th. Verstappen, Geomorphical reconnaissance of Sumatra and adjacent islands (Indonesia), Walters Noordhoff, Groningen (1973).
34. H. R. DeShon, E. R. Engdahl, C. H. Thurber, M. Brudzinski, *Geophys. Res. Lett.* **32**, L24307 (2005).
35. R. Bilham, E. R. Engdahl, N. Feldl, S. P. Satyabala, *Seismol. Res. Lett.* **76**, 299 (2005).
36. K. Sieh *et al.*, *Eos Trans. AGU* **86**, Abstract T31C-05 (2005).
37. L. Prawirodirdjo, Y. Bock, *J. Geophys. Res.* **109**, B08405 (2004).
38. J. R. Curray, *J. Asian Earth Sci.* **25**, 187 (2005).
39. W. H. F. Smith, D. T. Sandwell, *Science* **277**, 5334 (1997).
40. Shuttle Radar Topography Mission (SRTM) data (http://seamless.usgs.gov/).

41. This research was supported by the NSF, the Gordon and Betty Moore Foundation, and the Indonesian International Joint Research Program (RUTI). The National Geographic Channel and The Discovery Channel provided partial helicopter support. The captains and crews of Derazona Helicopters, the Mentawai Indah, the Saraina, and the Sariman Jadi provided expert transportation in the air and on the sea. Thanks to M. Chlieh, M. Tobita, and M. Meiner for helpful discussions and to J. Giberson and S. Healy for assistance with spatial data. Finally, we thank the people in the earthquake-affected region for their hospitality and willingness to share their observations. This is Caltech Tectonics Observatory contribution number 29.

Supporting Online Material

www.sciencemag.org/cgi/content/full/311/5769/1897/DC1
Figs. S1 to S10
Tables S1 and S2
References

14 November 2005; accepted 20 January 2006
10.1126/science.1122602

REPORTS

A Radio Pulsar Spinning at 716 Hz

Jason W. T. Hessels,[1]* Scott M. Ransom,[2] Ingrid H. Stairs,[3] Paulo C. C. Freire,[4] Victoria M. Kaspi,[1] Fernando Camilo[5]

We have discovered a 716-hertz eclipsing binary radio pulsar in the globular cluster Terzan 5 using the Green Bank Telescope. It is the fastest spinning neutron star found to date, breaking the 24-year record held by the 642-hertz pulsar B1937+21. The difficulty in detecting this pulsar, because of its very low flux density and high eclipse fraction (~40% of the orbit), suggests that even faster spinning neutron stars exist. If the pulsar has a mass less than twice the mass of the Sun, then its radius must be constrained by the spin rate to be <16 kilometers. The short period of this pulsar also constrains models that suggest that gravitational radiation, through an *r*-mode (Rossby wave) instability, limits the maximum spin frequency of neutron stars.

The majority of neutron stars are observed to rotate slower than a few times a second; however, those in binary systems can reach spin rates of hundreds of times a second through the transfer of angular momentum from their companion star (*1*, *2*). Some of these neutron stars, termed millisecond pulsars, are persistent radio sources whose emission is modulated at the star's spin frequency. Determining the maximum achievable rotation rate of a neutron star is important for a variety of astrophysical problems, ranging from understanding the behavior of matter at supra-nuclear densities to estimating the importance of neutron stars as gravitational wave sources for current and upcoming gravitational wave detectors. For more than 24 years, the 642-Hz pulsar B1937+21, which is the first millisecond pulsar ever found, has been the fastest spinning neutron star known (*3*). It has been argued that faster ones are exceedingly rare, if they exist at all (*4*).

Per unit mass, globular clusters (GCs) have many more millisecond pulsars than does the Galactic disk. This is due to the extremely high stellar densities in their cores (10^4 to 10^6 pc^{-3}), which promote the creation of binary systems (*5*) where a neutron star is spun-up (or "recycled")